

Dynamic Prompt Allocation and Tuning for Continual Test-Time Adaptation

Chaoran Cui^a, Yongrui Zhen^a, Shuai Gong^a, Chunyun Zhang^a, Hui Liu^a, Yilong Yin^b

^a*School of Computing and Artificial Intelligence, Shandong University of Finance and Economics, Jinan, China*

^b*School of Software, Shandong University, Jinan, China*

Abstract

Continual test-time adaptation (CTTA) has recently emerged to adapt a pre-trained source model to continuously evolving target distributions, which accommodates the dynamic nature of real-world environments. To mitigate the risk of catastrophic forgetting in CTTA, existing methods typically incorporate explicit regularization terms to constrain the variation of model parameters. However, they cannot fundamentally resolve catastrophic forgetting because they rely on a single shared model to adapt across all target domains, which inevitably leads to severe inter-domain interference. In this paper, we introduce learnable domain-specific prompts that guide the model to adapt to corresponding target domains, thereby partially disentangling the parameter space of different domains. In the absence of domain identity for target samples, we propose a novel dynamic Prompt Allocation and Tuning (PAINT) method, which utilizes a query mechanism to dynamically determine whether the current samples come from a known domain or an unexplored one. For known domains, the corresponding domain-specific prompt is directly selected, while for previously unseen domains, a new prompt is allocated. Prompt tuning is subsequently performed using mutual information maximization along with structural regularization. Extensive experiments on three benchmark datasets demonstrate the effectiveness of our PAINT method for CTTA. We have released our code at <https://github.com/Cadezzyr/PAINT>.

Keywords:

test-time adaptation, continual learning, catastrophic forgetting, prompt tuning

1. Introduction

Deep neural networks have demonstrated considerable success across a broad spectrum of visual recognition tasks. However, their impressive effectiveness is generally observed when the training data and test data share the same distribution. In real-world applications, we often encounter distribution shifts, posing a substantial barrier to the generalization of deep models. Consequently, numerous research efforts have been devoted to enhancing model robustness against distribution shifts. For example, domain adaptation (DA) [1] aims to transfer knowledge learned from a labeled source domain to an unlabeled target domain, while domain generalization (DG) [2] focuses on leveraging data from multiple source domains to learn a model that can generalize well to any out-of-distribution target domain.

Email addresses: crcui@sdufe.edu.cn (Chaoran Cui), yrzhen2000@163.com (Yongrui Zhen), gsh8210@163.com (Shuai Gong), zhangchunyun1009@126.com (Chunyun Zhang), liuh_lh@sdufe.edu.cn (Hui Liu), ylyin@sdu.edu.cn (Yilong Yin)

Both DA and DG methods require access to labeled source data. This requirement may be impractical due to privacy concerns and limitations in storage resources. We may only have access to a pre-trained source model, with the expectation that this model can effectively adapt to unlabeled target data at test time. This scenario is commonly referred to as test-time adaptation (TTA) [3]. TTA often needs to be conducted in an online manner, where target data is processed sequentially, and the model adapts to each new batch of data before making predictions. In online TTA, the model is prohibited from storing target data during adaptation [4].

Traditional TTA research [5, 6, 7] assumes that all target samples originate from the same stationary domain. In practice, however, the distribution of target samples can continuously change over time. For instance, an autonomous driving system must navigate through diverse road conditions, cope with varying weather, and handle unexpected scenarios. To accommodate this situation, continual test-time adaptation (CTTA) [8, 9] has been introduced, where the target test data is streamed from an environment that continuously evolves.

A major difficulty in CTTA is catastrophic forgetting [10], where the model forgets previously acquired knowledge as it continuously adapts to dynamic data distributions. To mitigate catastrophic forgetting, prior research typically incorporates an additional regularization term to constrain the variation of model parameters. For example, CoTTA [8] proposes to stochastically restore a small portion of parameters to their initial values from the pre-trained source model to help preserve source knowledge over the long term. EcoTTA [11] utilizes a self-distillation strategy to ensure that the output of the adaptation model does not deviate significantly from that of the source model. EATA [9] introduces a Fisher regularizer to prevent important model parameters from undergoing drastic changes.

Despite remarkable progress, existing methods may still fail to sufficiently address the issue of catastrophic forgetting. Their limitation lies in relying on a single shared model to adapt across all target domains, which inevitably introduces severe *inter-domain interference* [12]. When the shared model adapts to new target domains, its parameters are updated to optimize the performance on the new data. This process risks overwriting parameters that were crucial for previous domains, leading to catastrophic forgetting. Therefore, to fundamentally resolve catastrophic forgetting, it is essential to allow different domains to be learned in *a separated way* for CTTA.

In this paper, we draw inspiration from recent advances in prompt tuning for deep neural networks [13, 14]. Prompt tuning involves inserting a few learnable prompt tokens as extra inputs to facilitate the rapid adaptation of a pre-trained model to downstream tasks. By designing domain-specific prompts for individual target domains, we can partially disentangle the parameter space across different domains. Samples from a target domain contribute solely to optimizing their corresponding domain-specific prompts. In this way, the interference between domains can be significantly reduced, thereby minimizing catastrophic forgetting. However, realizing this idea in the context of CTTA presents a significant challenge: *the domain identity of target samples is unknown*. This uncertainty makes it difficult to determine which adaptation task is currently being processed and hinders the automatic selection of an appropriate prompt.

To tackle this challenge, we propose a novel dynamic Prompt Allocation and Tuning (PAINT) method for CTTA. Specifically, we maintain a memory buffer to store all domain-specific prompts, with each prompt

organized as a key-value pair. Initially, the memory buffer is empty and gradually expands as the target samples arrive. For each batch of target samples, we employ a query mechanism to dynamically determine whether the data comes from a known domain or an unexplored one. For known domains, we directly select the corresponding domain-specific prompt from the memory buffer. In cases of unseen domains, we allocate a new prompt in the memory buffer for that domain. Then, we perform prompt tuning following the principle of mutual information maximization [15], which improves both individual certainty and global diversity of the target predictions. Structural regularization is further incorporated to ensure consistency between the predictions on interpolated target samples and the interpolated sample labels [16], thereby enhancing the model’s generalization ability in the target domain. Beyond domain-specific prompts, we also fine-tune the shallow encoder blocks of the pre-trained model, which can be regarded as the common knowledge shared by all domains. Finally, the prompt key is updated using a simple moving average strategy.

It is important to note that, although some studies [14, 17] have explored prompt tuning in continual learning, they either predetermine the number of prompts or require explicit boundaries between different domains, which significantly differ from our PAINT method. To sum up, our main contributions are as follows:

- We recognize that catastrophic forgetting essentially stems from the inter-domain interference in CTTA. In contrast to prior research that rely on a single shared model to adapt across all target domains, we introduce domain-specific prompts to guide model adaptation, enabling the parameter space of different domains to be partially disentangled.
- Given the absence of domain identity for target samples, we design a query mechanism that dynamically determines whether to select an existing domain-specific prompt or to allocate a new prompt for the current samples. Prompt tuning is carried out using mutual information maximization along with structural regularization.
- Extensive experiments demonstrate the effectiveness of our PAINT method for CTTA, which achieves the state-of-the-art performance on three benchmark datasets.

The remainder of the paper is structured as follows: Section 2 provides a review of related work. Section 3 presents the preliminary knowledge of our study. Section 4 details our PAINT method for CTTA. Experimental results are discussed in Section 5, followed by the conclusions in Section 6.

2. Related Work

In this section, we first review the existing literature on TTA. Then, we present a brief overview of two closely related fields: continual learning and prompt tuning.

2.1. Test-Time Adaptation

TTA aims to adapt a pre-trained model from the source domain to unlabeled data in the target domain [3]. Fully TTA, which is often known as source-free domain adaptation [15], leverages all the target data to perform

adaptation before making any predictions. In contrast, online TTA [4] incrementally adapts the model as each target sample or small batch of samples is encountered. Numerous TTA methods have explored techniques such as self-training and entropy minimization for adapting the source model. For example, TENT [5] updates the model parameters in batch normalization layers via entropy minimization. CPL [18] proposes a conjugate pseudo labeling strategy to enhance self-training on the target domain.

CTTA refers to a scenario where the target domain undergoes continuous changes, presenting additional challenges for conventional TTA methods, particularly the risk of catastrophic forgetting. As the pioneering work, CoTTA [8] introduces a teacher-student pseudo-labeling framework augmented with stochastic weight restoration. RMT [19] further proposes to use symmetric cross-entropy as the consistency loss between the teacher and student models. EATA [9] and SAR [20] select reliable target samples and only use them to update the model for test-time adaptation. SANTA [21] leverages a self-distillation technique that regards the source model as an anchor to align target features.

Unlike these methods that rely on a shared model for all target domains, we exploit learnable domain-specific prompts to guide model adaptation, partially disentangling the parameter space across different domains.

2.2. *Continual Learning*

Continual learning (CL) [12], also known as lifelong learning, refers to the ability of a machine learning model to learn sequentially from a stream of data over time, without forgetting previously acquired knowledge. To address catastrophic forgetting, existing CL methods can be broadly classified into three categories: regularization-based methods [10, 22], which constrain updates to model parameters critical for earlier tasks; replay-based methods [23, 24], which replay stored or generated data from past tasks to maintain memory; and architecture-based methods [25, 26], which allocate separate parts of the model to individual tasks to prevent interference. Our PAINT method falls into architecture-based methods, but it introduces a novel query mechanism for dynamically allocating domain-specific prompts rather than permanently assigning fixed model components to individual tasks.

Recent studies, including L2P [14] and DualPrompt [27], have utilized learnable prompts to guide models in CL. PAINT distinguishes itself from these methods in two key aspects: 1) While these methods operate in a supervised manner, PAINT addresses the TTA problem by adapting the source model using unlabeled target samples; and 2) In contrast to these methods, which rely on a fixed number of prompts, PAINT flexibly adjusts the number of prompts as needed.

2.3. *Prompt Tuning*

As one of the most parameter-efficient fine-tuning techniques, prompt tuning was initially proposed in the field of natural language processing [28]. By inserting either templated or learnable prompt tokens into textual inputs, it enables the adaptation of pre-trained models to downstream tasks. CoOp [29] transforms the input textual contexts into learnable prompts for adapting vision-language models to few-shot image recognition. VPT [13] introduces a small set of visual prompt tokens into the vision transformer (ViT) [30]. Maple [31]

utilizes both text prompts and visual prompts to improve the alignment between paired textual and visual representations.

To facilitate CTTA, a recent study named VDP [17] introduces pixel-level prompts to decorate input images processed by convolutional neural networks (CNNs). It also develops domain-specific prompts, but is only applicable to scenarios with clearly defined domain boundaries, where target samples from different domains arrive in a strictly sequential manner [12]. Our PAINT method performs token-level prompt tuning based on transformer architecture. Different from VDP, PAINT eliminates the need for explicit domain boundaries by designing a dynamic query mechanism that allows target samples to determine the domains to which they belong.

3. Preliminaries

In this section, we first formulate the problem of CTTA. Then, we briefly describe the technique of visual prompt tuning.

3.1. Problem Definition

In CTTA, we are provided with a pre-trained model f_{Θ} with parameters Θ that has been trained on a source domain. Our goal is to adapt the pre-trained model to test samples from continuously evolving target domains in an online manner. The data distribution varies not only between the source domain and each target domain but also among different target domains. During adaptation, access to source data is restricted, and each test sample can be utilized only once.

Typically, test samples arrive sequentially in batches. Let $\mathcal{B} = \{\mathbf{x}_1, \mathbf{x}_2, \dots, \mathbf{x}_B\}$ denote a batch of samples from a certain target domain, where B is the batch size. The model needs to be adapted according to \mathcal{B} by updating the parameters Θ with one gradient step, and then make online predictions for each sample $\mathbf{x}_i \in \mathcal{B}$. *Note that we neither know the domain identity of test samples nor the total number of target domains.* As a common practice in CTTA, we consider the K -way image classification task and assume that different domains share the same category space.

3.2. Visual Prompt Tuning

CNN-based methods have dominated the field of CTTA for a long time. With the recent popularity of ViT [30] in numerous visual applications, ViT-based approaches [32] have started to show promising results in CTTA. We employ the visual prompt tuning technique [13] to adapt a pre-trained ViT model to new target domains with minimal computation cost. Given an input image \mathbf{x}_i , it is first divided into a sequence of fixed-size patches and projected into patch embeddings $\mathbf{E}_i \in \mathbb{R}^{L_e \times D_e}$, where L_e denotes the sequence length and D_e denotes the embedding dimension. Then, a learnable prompt $\mathbf{P} \in \mathbb{R}^{L_p \times D_e}$ that consists of L_p prompt tokens is prepended to the patch embeddings for guiding model adaptation. Conceptually, ViT can be decomposed into a feature encoder $\mathcal{F}(\cdot)$ comprising a stack of transformer blocks and a softmax classification head $\mathcal{H}(\cdot)$.

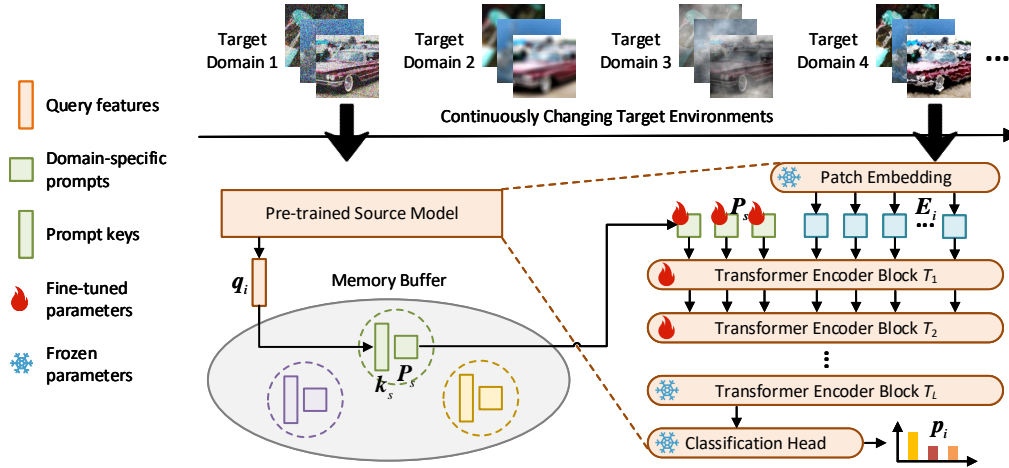


Figure 1: Conceptual framework of our PAINT method for CTTA.

The combined sequence $[\mathbf{P}; \mathbf{E}_i]$ is fed into the encoder to extract visual features $\mathbf{f}_i \in \mathbb{R}^{D_f}$, which are finally transformed into a class probability distribution $\mathbf{p}_i \in [0, 1]^K$ for the input \mathbf{x}_i :

$$\begin{aligned} \mathbf{f}_i &= \mathcal{F}([\mathbf{P}; \mathbf{E}_i]), \\ \mathbf{p}_i &= \mathcal{H}(\mathbf{f}_i). \end{aligned} \quad (1)$$

4. Method

To reduce the interference between domains, we propose a dynamic Prompt Allocation aNd Tuning (PAINT) method for CTTA. PAINT leverages a query mechanism to dynamically allocate a domain-specific prompt for incoming target samples, and integrates mutual information maximization with structural regularization for prompt tuning. The conceptual framework of PAINT is illustrated in Figure 1.

4.1. Dynamic Prompt Allocation

The domain identity of target samples is unknown at test time. To facilitate domain-specific prompt tuning, we aim to empower the samples themselves to decide which prompt to utilize through a query mechanism. For this purpose, we maintain a memory buffer $\mathcal{M} = \{(\mathbf{k}_1, \mathbf{P}_1), (\mathbf{k}_2, \mathbf{P}_2), \dots\}$ to store all domain-specific prompts, in which each prompt \mathbf{P}_j is regarded as a value and is associated with a key $\mathbf{k}_j \in \mathbb{R}^{D_f}$. Initially, the memory buffer \mathcal{M} is empty and gradually expands as the target samples arrive.

Specifically, upon receiving the batch of samples \mathcal{B} , we directly adopt the pre-trained source model as a frozen feature extractor to obtain the visual features $\mathbf{q}_i \in \mathbb{R}^{D_f}$ for each sample $\mathbf{x}_i \in \mathcal{B}$, i.e., $\mathbf{q}_i = \mathcal{F}(\mathbf{E}_i)$. The sample \mathbf{x}_i uses \mathbf{q}_i as a query and retrieves the most appropriate prompt by matching \mathbf{q}_i with each prompt key \mathbf{k}_j from the memory buffer. In our study, we empirically used the cosine similarity as the matching function, and the retrieval process can be expressed by

$$\mathbf{k}_s^i, \mathbf{P}_s^i = \arg \max_{(\mathbf{k}_j, \mathbf{P}_j) \in \mathcal{M}} \text{cosine}(\mathbf{q}_i, \mathbf{k}_j), \quad (2)$$

where $\text{cosine}(\cdot, \cdot)$ denotes the cosine similarity function, and \mathbf{P}_s^i denotes the prompt selected by \mathbf{x}_i and is paired with the key \mathbf{k}_s^i . During the prompt allocation, all samples in the batch can make their own choices,

and we aggregate their opinions via majority voting to reach a consensus on the optimal prompt for the batch of data:

$$\mathbf{k}_s, \mathbf{P}_s = \arg \max_{(\mathbf{k}_j, \mathbf{P}_j) \in \mathcal{M}} \sum_{i=1}^B \mathbb{1}(\mathbf{k}_j = \mathbf{k}_s^i), \quad (3)$$

where $\mathbb{1}(\cdot)$ is an indicator function that outputs 1 if the input argument is true and 0 otherwise.

It is worth noting that the domain-specific prompt \mathbf{P}_s selected by the majority of samples might not be ideal. This is because the samples probably come from a target domain that has not been encountered before. As a result, none of the prompts in the memory buffer correspond to the domain of the data. To overcome this issue, we compute the average matching score between all samples and \mathbf{k}_s to assess its reliability:

$$r_s = \frac{1}{B} \sum_{i=1}^B \text{cosine}(\mathbf{q}_i, \mathbf{k}_s). \quad (4)$$

Intuitively, if \mathbf{k}_s exhibits a high matching degree with the current samples, then \mathbf{P}_s can be considered a reliable prompt for the domain to which the samples belong. Conversely, insufficient matching suggests that the current samples are likely from an unexplored target domain. In this case, it becomes necessary to allocate a new prompt in the memory buffer for the domain. Therefore, we introduce a predefined threshold η . If r_s falls below η , the previously selected domain-specific prompt is discarded, and a new prompt is initialized in the memory buffer to serve as the selection for the current data:

$$\begin{aligned} \mathbf{k}_s &\leftarrow \frac{1}{B} \sum_{i=1}^B \mathbf{q}_i, \mathbf{P}_s \leftarrow \mathbf{Z}, & \text{if } r_s < \eta, \\ \mathcal{M} &\leftarrow \mathcal{M} \cup \{(\mathbf{k}_s, \mathbf{P}_s)\}, \end{aligned} \quad (5)$$

where $\mathbf{Z} \in \mathbb{R}^{L_p \times D_e}$ is a random matrix used for initialization. Note that for the first batch of samples, we directly initialize a new prompt, as the memory is empty at this stage.

4.2. Optimization Objective

After determining the domain-specific prompt \mathbf{P}_s suitable for the current batch of samples \mathcal{B} , we can further use \mathcal{B} to optimize \mathbf{P}_s . Existing CTTA methods primarily rely on entropy minimization [5] or a teacher-student pseudo-labeling scheme [8, 19] for model adaptation in unlabeled target domains. However, entropy minimization can lead to overly confident predictions, causing the model to collapse into a limited set of categories, while maintaining both a teacher and a student model requires additional computational resources. Besides, the intrinsic structural information [33] of the target domain remains underexplored in previous studies.

In this study, we aim to maximize the mutual information [15, 34] of the model’s predictions on target samples. The loss function for maximizing the mutual information is defined as follows:

$$\mathcal{L}_{mi} = \frac{1}{B} \sum_{i=1}^B H(\mathbf{p}_i) - H\left(\frac{1}{B} \sum_{i=1}^B \mathbf{p}_i\right), \quad (6)$$

where \mathbf{p}_i is the model’s predicted probability distribution for the target sample $\mathbf{x}_i \in \mathcal{B}$, and $H(\mathbf{p}_i) = -\sum_{k=1}^K p_i^k \log p_i^k$ denotes the entropy function with p_i^k being the k -th element of \mathbf{p}_i . The first term of Eq. (6) is

the average entropy of the model’s predictions, and minimizing it prevents the model from producing ambiguous predictions for individual target samples. The second term is the negative entropy of the average output of the model, and minimizing it improves prediction diversity within a batch, thereby reducing the risk of the model’s predictions collapsing into a few categories. By combining the two terms, the mutual information loss \mathcal{L}_{mi} contributes to both individual prediction certainty and overall prediction diversity for the target data.

We also incorporate structural regularization to ensure consistency between the model’s predictions on interpolated target samples and the interpolated sample labels [16]. Let $\hat{\mathbf{p}}_i$ denote the category distribution predicted by the model for \mathbf{x}_i prior to batch optimization, i.e., by the model using the domain-specific prompt \mathbf{P}_s before being updated. The pseudo label \hat{y}_i for \mathbf{x}_i is generated based on $\hat{\mathbf{p}}_i$ if the prediction confidence exceeds a threshold ϕ :

$$\hat{y}_i = \arg \max_k \hat{p}_i^k, \text{ if } \max_k \hat{p}_i^k > \phi. \quad (7)$$

Then, each pair of target samples assigned with pseudo labels $\mathbf{x}_i, \mathbf{x}_j \in \mathcal{B}$ is randomly mixed, and their pseudo labels are correspondingly mixed:

$$\begin{aligned} \mathbf{x}_{ij} &= \lambda \mathbf{x}_i + (1 - \lambda) \mathbf{x}_j, \\ \hat{y}_{ij} &= \lambda \hat{y}_i + (1 - \lambda) \hat{y}_j, \end{aligned} \quad (8)$$

where $\lambda \sim \text{Beta}(\alpha, \alpha)$ with α set to 1.0, ensuring that the interpolation coefficient λ is uniformly distributed over the interval $[0, 1]$. Denote by \mathbf{p}_{ij} the model’s prediction on the blended sample \mathbf{x}_{ij} . The interpolation consistency regularization can be formulated as the cross-entropy loss between \mathbf{p}_{ij} and \hat{y}_{ij} :

$$\mathcal{L}_{ic} = -\frac{1}{B} \sum_{\mathbf{x}_i, \mathbf{x}_j \in \mathcal{B}} \log(p_{ij}^{\hat{y}_{ij}}). \quad (9)$$

Intuitively, \mathcal{L}_{ic} compels the model to predict not only on the original target samples but also across the interpolated regions between them, thereby enhancing the model’s generalization ability in the target domain.

Overall, the ultimate optimization objective of our PAINT method is as follows:

$$\min \mathcal{L}_{mi} + \beta \mathcal{L}_{ic}, \quad (10)$$

where β is a hyperparameter balancing mutual information loss and interpolation consistency loss. In addition to the domain-specific prompt \mathbf{P}_s , we fine-tune the feature encoder $\mathcal{F}(\cdot)$ of the pre-trained model using the objective in Eq. (10). To maintain a relatively low computational overhead, only the first three blocks of $\mathcal{F}(\cdot)$ are updated during training. These shallow blocks capture the common knowledge shared by all target domains. While this idea could also be implemented by inserting domain-invariant prompts into the model [17, 27], our experiments revealed that this option is less effective than fine-tuning the shallow encoder blocks.

4.3. Prompt Key Updating

If the prompt key \mathbf{k}_s is not newly initialized as shown in Eq. (5), we update \mathbf{k}_s using a moving average approach, aligning it with the average query features of the corresponding target domain:

$$\mathbf{k}_s \leftarrow \gamma \mathbf{k}_s + \frac{(1 - \gamma)}{B} \sum_{i=1}^B \mathbf{q}_i, \quad (11)$$

Algorithm 1 Pseudocode of model adaptation in PAINT.

Input:

Target samples arriving sequentially in batches, a pre-trained source model, and hyperparameters

Initialization:

A memory buffer $\mathcal{M} = \emptyset$.

1: **for** each batch of samples $\mathcal{B} = \{\mathbf{x}_1, \mathbf{x}_2, \dots, \mathbf{x}_B\}$ **do**

2: /* Prompt allocation */

3: **if** $\mathcal{M} == \emptyset$ **then**

4: Allocate a new prompt $(\mathbf{k}_s, \mathbf{P}_s)$ in \mathcal{M} ; // Eq. (5)

5: **else**

6: **for** each sample $\mathbf{x}_i \in \mathcal{B}$ **do**

7: Extract the query features \mathbf{q}_i and retrieve the best-matching prompt $(\mathbf{k}_s^i, \mathbf{P}_s^i)$ for \mathbf{x}_i ; // Eq. (2)

8: **end for**

9: Select the optimal prompt $(\mathbf{k}_s, \mathbf{P}_s)$ for \mathcal{B} via majority voting; // Eq. (3)

10: Compute the reliability r_s of $(\mathbf{k}_s, \mathbf{P}_s)$; // Eq. (4)

11: **if** $r_s < \eta$ **then**

12: Discard the selected prompt $(\mathbf{k}_s, \mathbf{P}_s)$;

13: Allocate a new prompt $(\mathbf{k}_s, \mathbf{P}_s)$ in \mathcal{M} ; // Eq. (5)

14: **end if**

15: **end if**

16: /* Prompt tuning */

17: **for** each sample $\mathbf{x}_i \in \mathcal{B}$ **do**

18: Predict the class distribution \mathbf{p}_i for \mathbf{x}_i ; // Eq. (1)

19: Generate the pseudo label \hat{y}_i for \mathbf{x}_i ; // Eq. (7)

20: **end for**

21: Compute the mutual information loss \mathcal{L}_{mi} and the interpolation consistency loss \mathcal{L}_{ic} ; // Eq. (6) and Eq. (9)

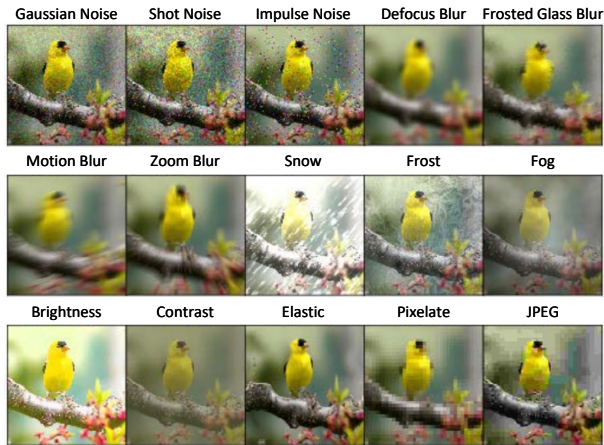
22: Optimize the prompt value \mathbf{P}_s and the shallow blocks of $\mathcal{F}(\cdot)$ based on \mathcal{L}_{mi} and \mathcal{L}_{ic} ; // Eq. (10)

23: Update the prompt key \mathbf{k}_s using a moving average strategy; // Eq. (11)

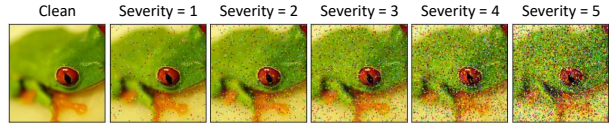
24: **end for**

where γ is a smoothing coefficient fixed at 0.8 to prevent dramatic fluctuations in the moving average. In this manner, \mathbf{k}_s is consistently refined and eventually stabilizes to achieve an alignment with the target domain.

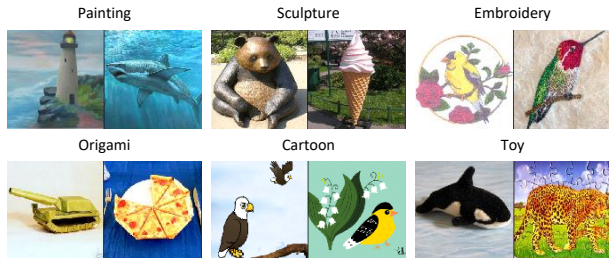
For clarity, we present the pseudocode of model adaptation in our PAINT method in Algorithm 1. In particular, Lines 3-15 describe the prompt allocation process via the dynamic query mechanism, while Lines 17-23 summarize the steps of prompt tuning.



(a) 15 corruption types applied to images.



(b) Corrupted images at five severity levels.



(c) Example images in different artistic renditions.

Figure 2: Images with various corruption types and severity levels on CIFAR10-C and ImageNet-C, as well as some examples in different artistic renditions from ImageNet-R. The images are sourced from [35] and [36], respectively.

5. Experiments

In this section, we provide a detailed description of the experimental settings and present a series of experimental results to demonstrate the effectiveness of our PAINT method.

5.1. Datasets

We conducted experiments on three benchmark datasets for out-of-distribution evaluation, i.e., CIFAR10-C, ImageNet-C, and ImageNet-R.

CIFAR10-C and ImageNet-C [35] are corrupted versions of the original CIFAR10 and ImageNet datasets, respectively. They are designed to evaluate model robustness against various common corruptions and perturbations. CIFAR10-C introduces a series of corruptions to the test set of CIFAR10 (10,000 images across 10 categories), while ImageNet-C applies these corruptions to the validation set of ImageNet (50,000 images across 1,000 categories). Both datasets contain a total of 15 distinct corruption types, grouped into four main categories: noise, blur, weather, and digital. Each corruption type is applied at five different severity levels, ranging from mild to severe. This setup facilitates the study of how models perform under gradually worsening conditions.

ImageNet-R [36] is a variant of the ImageNet dataset specifically crafted to evaluate the robustness of image classifiers to domain shifts caused by artistic renditions. Unlike the traditional corruptions in CIFAR10-C and ImageNet-C, ImageNet-R focuses on shifts that arise from different visual styles and representations. The dataset comprises 30,000 images from 200 ImageNet classes, with objects depicted in various artistic forms, such as paintings, cartoons, graffiti, embroidery, and sculptures. Figure 2 shows the images with varying corruption types and severity levels on CIFAR10-C and ImageNet-C, as well as some examples in different artistic renditions from ImageNet-R.

Method	Noise			Blur				Weather				Digital				Avg.
	Gauss.	Shot	Impul.	Defoc.	Glass	Motion	Zoom	Snow	Frost	Fog	Brit.	Contr.	Elastic	Pixel	JPEG	
WideResNet-28	27.70	34.30	27.10	53.10	45.70	65.20	58.00	74.90	58.70	74.00	90.70	53.30	73.40	41.50	69.70	56.50
• CoTTA	75.70	78.70	73.40	88.40	72.40	87.80	89.70	85.20	85.90	87.60	92.50	89.40	81.70	86.60	82.70	83.80
• EATA	75.70	80.70	72.40	87.40	71.40	85.60	88.00	84.10	85.40	84.60	90.40	86.70	79.40	83.70	78.20	82.20
• TENT	75.20	79.40	71.40	85.60	68.90	83.50	85.90	80.90	81.40	81.40	87.80	79.70	74.30	79.20	75.10	79.30
• VDP	77.40	80.30	71.90	92.90	71.60	90.50	93.70	89.80	88.50	91.00	98.50	94.40	81.50	87.20	81.50	86.00
• SANTA	76.10	79.90	72.00	88.40	72.60	87.40	89.80	85.90	86.80	87.80	92.60	89.70	80.90	86.70	81.50	83.90
• RMT	75.50	80.00	74.50	86.10	75.40	85.10	86.70	84.00	84.20	84.40	88.90	85.00	81.70	85.40	83.10	82.70
ViT-B/16	77.10	79.38	81.75	88.06	67.58	84.12	89.58	92.41	90.54	81.98	96.47	65.56	79.83	63.46	80.50	81.22
• CoTTA	77.10	79.39	81.74	88.07	67.56	84.12	89.58	92.41	90.57	81.97	96.48	65.58	79.90	63.48	80.49	81.23
• ETA	78.09	80.26	82.28	88.26	67.63	84.48	89.69	92.43	90.66	82.17	96.48	66.52	80.12	62.88	80.69	81.51
• CPL	83.52	88.25	89.20	91.47	78.55	90.67	94.08	94.37	94.66	91.61	97.21	93.11	87.45	88.01	88.01	90.01
• RMT	80.97	85.88	86.68	90.57	85.71	90.07	93.83	93.84	94.47	91.67	96.31	91.95	89.80	91.62	89.93	90.35
• SAR	85.46	85.74	88.64	90.79	80.57	89.10	90.90	92.40	91.11	88.92	96.48	86.88	85.27	76.73	85.63	87.64
• PAINT	86.26	89.08	90.56	93.48	84.21	92.75	95.20	94.55	95.23	94.43	96.85	95.90	89.14	92.94	89.43	92.00

Table 1: Classification accuracy on CIFAR10-C at the highest corruption severity level. Each column represents the performance on a target domain, with data from different target domains arriving sequentially from left to right.

5.2. Evaluation Protocol

Following previous work [8], we continuously adapted the pre-trained source model to the test samples from different target domains that arrived sequentially without resetting the model. The model was updated with one gradient step for each batch of samples and then made predictions on them immediately. On CIFAR10-C and ImageNet-C, each corruption type at its highest severity level corresponds to an individual target domain, while various rendition styles are regarded as target domains on ImageNet-R. We employed the models trained on the original CIFAR10 and ImageNet as our pre-trained source models. For each dataset, we evaluated the classification accuracy for each target domain, as well as the average accuracy across different domains.

5.3. Baselines

We compared PAINT with several recently proposed CTTA methods based on ResNet and ViT backbones. The baseline methods include CoTTA [8], EATA [9], ETA [9], TENT [5], SANTA [21], VDP [17], CPL [18], RMT [19], and SAR [20]. A concise overview of these methods has been presented in Section 2. For ResNet-based baselines, we directly cited the results from their original papers or other published papers [37] if available. As the results of all ViT-based baselines were not reported in existing literature, we reproduced these methods, strictly adhering to the hyperparameters specified in their original papers.

5.4. Implementation Details

We followed the experimental setups described in previous CTTA studies [8, 9]. All input images were resized to 224×224 and normalized to the range $[0, 1]$. The random seed was fixed at 0 for all methods during training. All experiments were conducted in PyTorch using a single NVIDIA GeForce RTX 3090 GPU and 128GB system memory.

For PAINT, we employed the pre-trained ViT-B/16 source model for prompt tuning, where the dimensions of both the patch embeddings and visual features are 768. During adaptation, the batch size and learning

Method	Noise			Blur				Weather				Digital				Avg.
	Gauss.	Shot	Impul.	Defoc.	Glass	Motion	Zoom	Snow	Frost	Fog	Brit.	Contr.	Elastic	Pixel	JPEG	
ResNet-50	2.20	2.90	1.80	17.80	9.80	14.50	22.50	16.80	23.40	24.60	59.00	5.50	17.10	20.70	31.60	18.00
• CoTTA	15.30	17.90	19.40	18.70	21.00	31.40	42.50	39.70	39.50	51.70	63.40	33.90	52.80	58.80	54.00	37.30
• EATA	35.00	38.10	36.80	33.80	34.20	47.30	53.20	51.10	45.60	59.70	68.00	44.20	57.20	60.40	54.70	47.95
• TENT	18.40	25.40	27.30	22.40	26.20	34.50	44.70	38.40	37.00	48.30	61.80	27.90	49.20	52.60	46.70	37.40
• SANTA	25.90	27.10	28.40	24.30	25.90	35.80	44.50	44.40	37.10	53.40	63.90	30.10	49.40	55.70	51.50	39.90
• RMT	19.80	23.60	25.50	22.90	25.60	33.80	42.40	43.00	40.90	52.00	60.90	39.40	52.70	57.50	56.60	39.80
ViT-B/16	46.90	45.80	47.00	31.35	21.30	42.30	38.20	49.55	45.40	43.45	74.45	9.00	41.85	62.15	64.65	44.22
• CoTTA	50.48	56.42	58.32	39.48	42.50	52.02	46.76	56.92	59.84	53.12	70.98	15.74	62.58	68.26	67.54	53.40
• ETA	56.02	60.40	58.60	46.96	46.40	53.48	53.94	56.78	59.44	58.00	74.52	37.26	55.76	64.88	65.96	56.56
• CPL	51.30	57.60	57.46	44.18	42.02	54.16	51.06	60.88	58.98	59.58	76.10	47.28	28.68	47.06	2.48	49.25
• RMT	49.28	52.70	55.28	40.38	40.98	51.54	48.30	56.64	56.72	53.70	69.66	26.64	62.46	68.56	68.20	53.41
• SAR	56.22	60.48	59.30	48.64	50.06	55.46	54.50	59.88	60.82	60.22	75.94	45.04	57.76	68.20	68.40	58.73
• PAINT	54.34	58.16	58.14	50.18	50.54	57.62	55.66	62.46	63.00	65.92	77.58	53.30	56.22	71.94	69.66	60.31

Table 2: Classification accuracy on ImageNet-C at the highest corruption severity level.

Method	Art	Cart.	Dev.	ImageNet-C				ImageNet-R				ImageNet-V				Avg.
				Emb.	Graf.	Graphic	Misc	Orig.	Paint	Sculp.	Sketch	Stick.	Tat.	Toy	Video	
ViT-B/16	50.72	25.17	57.33	31.86	32.09	43.17	48.18	34.18	68.04	44.15	35.50	34.06	29.89	42.62	53.38	42.02
• CoTTA	51.31	27.99	61.26	34.49	35.39	50.47	55.74	40.91	74.85	54.52	56.62	39.37	39.29	51.62	63.92	49.18
• ETA	53.53	37.63	70.37	45.15	46.12	60.56	63.46	53.45	78.98	60.70	67.65	47.64	50.44	55.13	64.56	57.02
• CPL	37.17	14.20	43.09	19.94	19.98	29.81	35.80	20.73	53.90	30.77	25.10	18.70	20.08	28.39	30.87	28.57
• RMT	52.29	29.09	63.15	34.07	33.90	50.47	56.13	38.91	73.97	52.76	55.78	39.76	41.55	52.02	63.50	49.16
• SAR	51.05	26.22	59.08	32.27	33.16	45.65	51.21	35.45	70.62	46.99	44.89	37.20	33.90	46.13	57.17	44.73
• PAINT	57.33	42.70	71.94	54.02	51.33	58.07	64.46	60.91	76.58	61.20	65.84	45.67	50.39	55.20	62.38	58.53

Table 3: Classification accuracy on ImageNet-R.

rate were configured as 50 and 0.05, respectively. We set the prompt length L_p to 2, consistent with previous works [31]. The matching score threshold η and prediction confidence threshold ϕ were set to 0.2 and 0.6, respectively. For the loss balancing hyperparameter β , we chose $\beta = 1$. The impact of various hyperparameters on model performance will be discussed later. For the sake of reproducibility, the code of our PAINT method has been released at <https://github.com/Cadezzyr/PAINT>.

5.5. Performance Comparison

Results on CIFAR10-C. As shown in Table 1, the ViT-based source model is much better than its ResNet-based counterpart on CIFAR10-C, demonstrating the superior transferability of ViT. However, the source models exhibit relatively low accuracy and fall behind nearly all CTTA methods, indicating the necessity for model adaptation during testing. Our PAINT method achieves the highest performance in 11 out of the 15 target domains. It exceeds the source model and the second-best CTTA method RMT in average accuracy by 10.78% and 1.65%, respectively.

Results on ImageNet-C. As illustrated in Table 2, all CTTA methods demonstrate increasingly pronounced advantages over the source models on ImageNet-C. PAINT not only outperforms the other methods in average accuracy, but also emerges as the sole method to achieve a result exceeding 60%. Notably, when

	Source	CoTTA	ETA	CPL	RMT	SAR	PAINT
Accuracy	91.31 ± 0.00	91.35 ± 0.19	91.39 ± 0.17	95.59 ± 0.12	95.67 ± 0.40	92.96 ± 0.02	96.67 ± 0.14

Table 4: Performance comparison between different methods on CIFAR10C in the gradually changing scenario. We report the mean and standard deviation of average accuracy over ten shuffled sequences of target domains.

tackling the adaptation task in the ‘‘Contr.’’ domain, the ViT-based source model achieves an accuracy of only 9.00%. In contrast, PAINT shows significant superiority with an improvement of at least 6.02%, indicating its greater proficiency in addressing the most challenging tasks compared to the other methods.

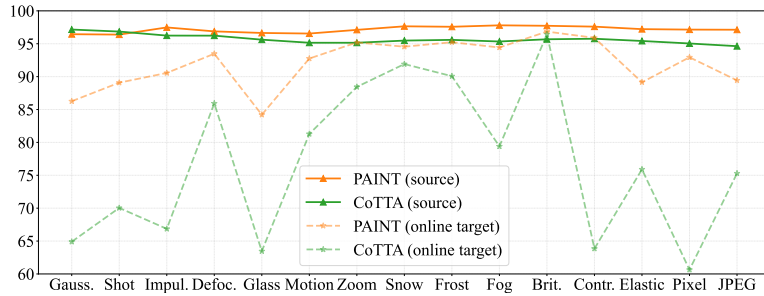
Results on ImageNet-R. Table 3 presents the results of all ViT-based methods on ImageNet-R. As expected, PAINT once again obtains the best performance, improving the average accuracy of the source model from 42.02% to 58.53%. It beats the runner-up method ETA by 1.51%. These results confirm the effectiveness of PAINT in mitigating continuous domain shifts for CTTA.

5.6. Comparison in Gradually Changing Scenario

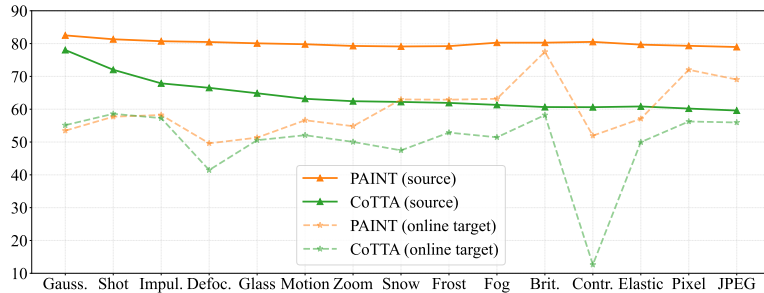
In CTTA, some domain shifts may gradually evolve over time, leading to the gradually changing scenario [19]. Following prior work [8], we simulate this scenario on CIFAR10-C by constructing sequences of target domains with progressively changing severity across the 15 corruption types: $\underbrace{\dots 2 \rightarrow 1}_{t-1 \text{ and before}} \xrightarrow{\text{type change}} \underbrace{1 \rightarrow 2 \rightarrow \dots}_{t+1 \text{ and on}}$, where the severity within each corruption type t increases from the lowest (1) to the highest (5) before returning to the lowest. On CIFAR10-C, each corruption type is regarded as an individual target domain. We performed ten independent random shuffles of the target domain sequence and computed the mean and standard deviation of the average accuracy across these shuffled sequences. As demonstrated in Table 4, our PAINT method still surpasses the other methods in the gradually changing scenario, achieving a mean average accuracy of 96.67% with a relatively low standard deviation of 0.14%. This corresponds to a 5.36% and 5.32% improvement in the mean value compared to the source model and CoTTA, respectively. Notably, compared to adapting to domains with only the highest severity level (see Table 1), adapting to target domains with lower severity levels consistently yields better results for all methods.

5.7. Anti-Forgetting Capability Test

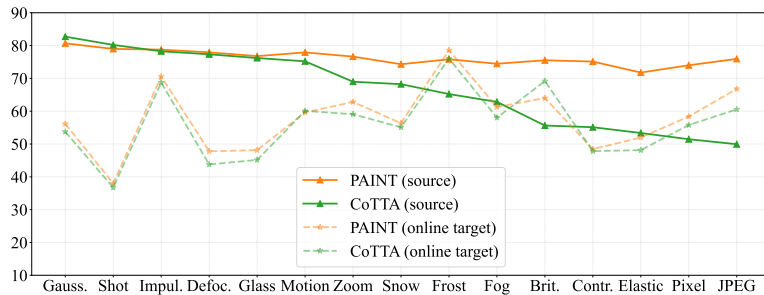
Following previous studies [9], we examined the anti-forgetting capability of our PAINT method by monitoring the model’s performance changes on the original source data during test-time adaptation. In Figure 3a, we compare the accuracy of PAINT with that of CoTTA on the source data of CIFAR10-C. As can be seen, although both models maintain over 95% accuracy on the clean source data, CoTTA’s accuracy slightly declines over time, while PAINT exhibits more stable performance. Figure 3b illustrates their comparison results on ImageNet-C. PAINT consistently outperforms CoTTA in every online target domain as well as the source domain during adaptation. Meanwhile, it is clear that CoTTA suffers from significant catastrophic forgetting, with its accuracy on the source data gradually decreasing from 78.04% to 59.60% over time. Comparatively,



(a) Classification accuracy on the source domain on CIFAR10-C.



(b) Classification accuracy on the source domain on ImageNet-C.



(c) Classification accuracy on the source domain on ImageNet-R.

Figure 3: Anti-forgetting capabilities of PAIN T and CoTTA.

PAIN T exhibits more stable performance in the source domain, with accuracy consistently maintaining around 80%. Figure 3c presents the comparison results on ImageNet-R. A similar trend can be observed, where CoTTA is even slightly ahead of PAIN T at the beginning; however, as model adaptation progresses, its accuracy in the source domain declines rapidly and eventually lags behind PAIN T by as much as 26 percentage points. Note that throughout testing, PAIN T seeks to allocate a distinct domain-specific prompt to all source data via the dynamic query mechanism. In this way, the source domain and target domains can be learned independently, thereby mitigating the inter-domain interference. The above results verify that PAIN T is more effective at preserving source knowledge and demonstrates a stronger ability to prevent catastrophic forgetting.

5.8. Ablation Study

Table 5 lists the results of several variants of our PAIN T method on ImageNet-C when different key components are omitted. In PAIN T, we perform test-time model adaptation by jointly optimizing the mutual information loss \mathcal{L}_{mi} and the interpolation consistency loss \mathcal{L}_{ic} . We can see that optimizing \mathcal{L}_{mi} alone out-

\mathcal{L}_{ent}	\mathcal{L}_{mi}	\mathcal{L}_{ic}	\mathbf{P}_s	$\mathcal{F}(\cdot)$	Accuracy
✓	✗	✗	✓	✓	47.45
✗	✓	✗	✓	✓	52.97
✗	✓	✓	✓	✓	60.31
✗	✓	✓	✗	✓	58.58
✗	✓	✓	✓	✗	59.46

Table 5: Contribution of different components of PAINT.

β	0.01	0.1	1	10	100
Accuracy	54.96	58.25	60.31	59.61	58.69

Table 6: Effect of the balancing hyperparameter β .

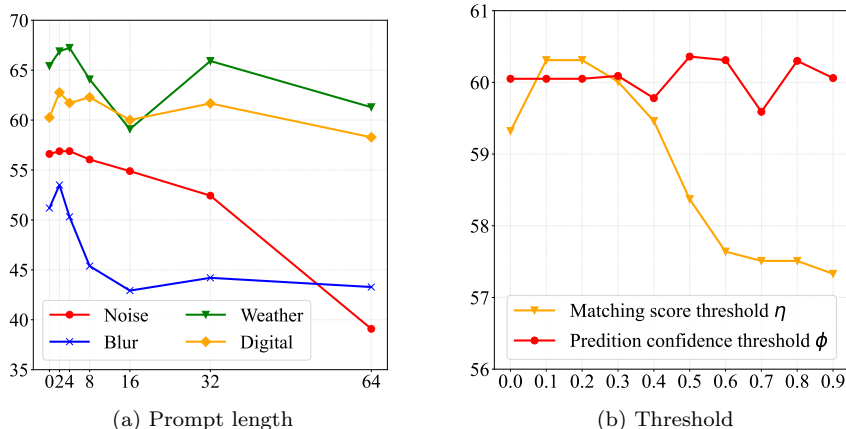


Figure 4: Effects of the prompt length and thresholds.

performs the traditional entropy minimization loss \mathcal{L}_{ent} [5], with performance gains that are further magnified when \mathcal{L}_{ic} is incorporated. These observations validate the rationality of our choice of optimization objective in PAINT. As previously mentioned, PAINT simultaneously updates the domain-specific prompt \mathbf{P}_s and the domain-agnostic shallow blocks of feature encoder $\mathcal{F}(\cdot)$ during adaptation. The variants that do not include either \mathbf{P}_s or $\mathcal{F}(\cdot)$ yield inferior results compared to PAINT, leading to a 1.73% and 0.85% drop in average accuracy, respectively. This finding indicates that learning both domain-specific and domain-agnostic knowledge are crucial for enhancing model performance.

5.9. Hyperparameter Analysis

We evaluate the influence of different hyperparameters on PAINT’s performance on ImageNet-C:

Effect of Prompt Length. Figure 4a shows the impact of prompt length across four corruption categories in target domains: We notice that the best results are achieved with short prompts (e.g., two or four prompt tokens), while further extending the length severely degrades model performance. One possible explanation is that longer prompts introduce additional model parameters. In CTTA, the model must make predictions immediately after being updated with a small amount of data in a batch. The increase in model parameters may lead to overfitting, particularly in an environment where the distribution of test data is continuously evolving.

	Prompt number	Matching accuracy	Classification accuracy
PAINT-Query	11	53.33	60.31
PAINT-Oracle	15	100	60.55

Table 7: Comparison between PAINT with our query mechanism (i.e., PAINT-Query) and a variant with perfect knowledge of the domain identity of target samples at test time (i.e., PAINT-Oracle) on ImageNet-C.

Effect of Threshold. Figure 4b depicts how the threshold hyperparameters η and ϕ affect PAINT’s performance. In Eq. (5), η represents the threshold for query and key matching scores in prompt allocation. It is observed that the performance goes down gradually when η exceeds 0.2. A higher value of η increases the likelihood of allocating a new prompt to each batch of samples. This can result in samples from the same target domain failing to share a consistent domain-specific prompt, thereby reducing the model’s accuracy. In Eq. (7), ϕ denotes the confidence threshold for the pseudo labels of target samples. The best results are obtained when $\phi = 0.5$ or $\phi = 0.6$. Overall, the performance of PAINT remains relatively stable as ϕ varies.

Effect of Loss Weight. In Eq. (10), the hyperparameter β controls the trade-off between the mutual information loss and the interpolation consistency loss. Table 6 displays the results obtained by PAINT with different values of β . We adjust β over several orders of magnitude ranging from 0.01 to 100. The performance improves progressively as β changes from 0.01 to 1, but deteriorates with any further increase.

5.10. Relationship between Query Accuracy and Model Performance

As described in Section 4.1, our PAINT method utilizes a query mechanism that dynamically determine whether to select an existing domain-specific prompt or to allocate a new prompt for each batch of target samples. To investigate the relationship between query accuracy and model performance, we compare PAINT against a variant in which the domain identity of target samples is provided at test time on ImageNet-C. The comparison results are presented in Table 7. We observe that in PAINT’s query mechanism, the matching accuracy between target samples and their true corresponding domain-specific prompts is not very high, at only 53.33%. For the 15 target domains on ImageNet-C, PAINT allocates only 11 prompts throughout the entire adaptation process. Remarkably, despite this mismatch, PAINT remains robust, with its performance using the query mechanism only being slightly behind that of the variant where the domain identity of target samples is known (60.31% versus 60.55%). We suspect that this robustness stems from the strong similarities between different target domains. For example, as illustrated in Table 2, multiple target domains often belong to the same corruption category. Since the matching is performed based on the visual features of target samples, PAINT can implicitly leverage domain similarities. Even if a mismatch occurs, PAINT may still select a prompt from a visually similar target domain, enabling it to achieve reasonable performance.

5.11. Visualization

To gain deeper insight into the superiority of our PAINT method, we visualize the class activation maps (CAMs) [38] generated by the source model, CoTTA, and PAINT for several corrupted images in target

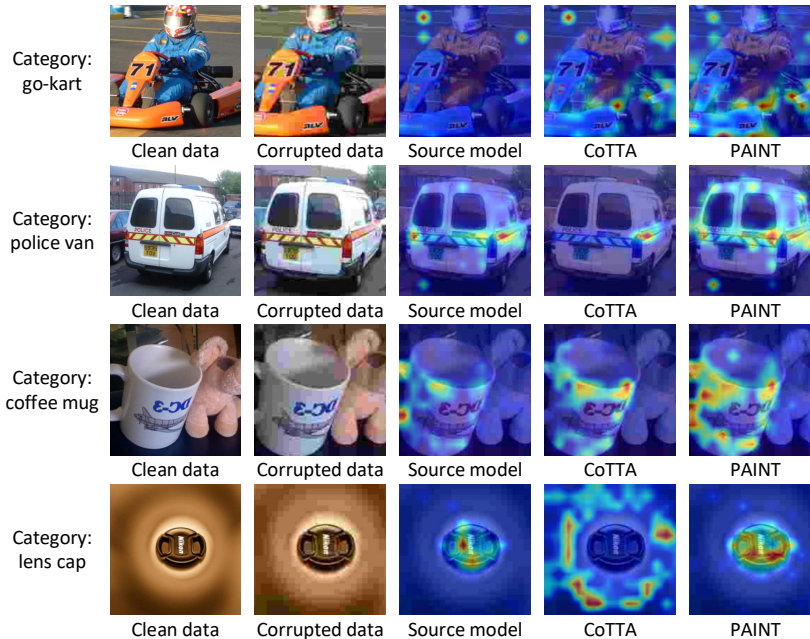


Figure 5: Visualization of attention maps learned by the source model, CoTTA, and PAINt for some corrupted images in target domains. Each image is annotated with its category label and paired with its corresponding clean image in the source domain.

domains on ImageNet-C. To generate these CAMs, we first compute the model’s output logits and use their gradients to weight the attention maps of each encoder block. The final CAMs are derived by averaging the weighted attention maps across all blocks. Figure 5 presents these visualizations, where each image is annotated with its category label and paired with its corresponding clean image in the source domain. It can be observed that PAINt focuses more accurately on the object of interest compared to the source model and CoTTA, effectively minimizing distractions from the background or unrelated objects. In contrast, CoTTA occasionally fails to adapt the source model. For example, for the image of the lens cap category, CoTTA diverts the source model’s attention to incorrect regions, whereas PAINt further refines the focus on important visual areas.

6. Conclusion

Catastrophic forgetting poses a significant challenge to CTTA, and it primarily stems from inter-domain interference. In this paper, we introduce domain-specific prompts that guide model adaptation, facilitating the partial disentanglement of parameter spaces across different domains. As the domain identity for target samples is unknown, we use a query mechanism to dynamically infer if data comes from a previously seen or new domain, followed by prompt tuning via mutual information maximization and structural regularization. Experiments on three benchmark datasets demonstrate the effectiveness of our PAINt method. One limitation of our current study lies in the assumption that the source and target domains share an identical category space, which may not hold in practice. Future work will explore extending PAINt to the open-set TTA setting [39], where target domains may contain samples from unknown categories.

References

- [1] G. Wilson, D. J. Cook, A survey of unsupervised deep domain adaptation, *ACM Transactions on Intelligent Systems and Technology* 11 (5) (2020) 1–46.
- [2] K. Zhou, Z. Liu, Y. Qiao, T. Xiang, C. C. Loy, Domain generalization: A survey, *IEEE Transactions on Pattern Analysis and Machine Intelligence* 45 (4) (2023) 4396–4415.
- [3] J. Liang, R. He, T. Tan, A comprehensive survey on test-time adaptation under distribution shifts, *arXiv preprint arXiv:2303.15361* (2023).
- [4] Y. Su, X. Xu, T. Li, K. Jia, Revisiting realistic test-time training: Sequential inference and adaptation by anchored clustering regularized self-training, *IEEE Transactions on Pattern Analysis and Machine Intelligence* 46 (8) (2024) 5524–5540.
- [5] D. Wang, E. Shelhamer, S. Liu, B. Olshausen, T. Darrell, Tent: Fully test-time adaptation by entropy minimization, in: *Proceedings of the 9th International Conference on Learning Representations*, 2021.
- [6] Y. Iwasawa, Y. Matsuo, Test-time classifier adjustment module for model-agnostic domain generalization, *Advances in Neural Information Processing Systems* 34 (2021) 2427–2440.
- [7] D. Chen, D. Wang, T. Darrell, S. Ebrahimi, Contrastive test-time adaptation, in: *Proceedings of the IEEE/CVF Conference on Computer Vision and Pattern Recognition*, 2022, pp. 295–305.
- [8] Q. Wang, O. Fink, L. Van Gool, D. Dai, Continual test-time domain adaptation, in: *Proceedings of the IEEE/CVF Conference on Computer Vision and Pattern Recognition*, 2022, pp. 7201–7211.
- [9] S. Niu, J. Wu, Y. Zhang, Y. Chen, S. Zheng, P. Zhao, M. Tan, Efficient test-time model adaptation without forgetting, in: *Proceedings of the 39th International Conference on Machine Learning*, 2022, pp. 16888–16905.
- [10] J. Kirkpatrick, R. Pascanu, N. Rabinowitz, J. Veness, G. Desjardins, A. A. Rusu, K. Milan, J. Quan, T. Ramalho, A. Grabska-Barwinska, et al., Overcoming catastrophic forgetting in neural networks, *Proceedings of the National Academy of Sciences* 114 (13) (2017) 3521–3526.
- [11] J. Song, J. Lee, I. S. Kweon, S. Choi, Ecotta: Memory-efficient continual test-time adaptation via self-distilled regularization, in: *Proceedings of the IEEE/CVF Conference on Computer Vision and Pattern Recognition*, 2023, pp. 11920–11929.
- [12] L. Wang, X. Zhang, H. Su, J. Zhu, A comprehensive survey of continual learning: Theory, method and application, *IEEE Transactions on Pattern Analysis and Machine Intelligence* (2024) 1–20 [doi:10.1109/TPAMI.2024.3367329](https://doi.org/10.1109/TPAMI.2024.3367329).
- [13] M. Jia, L. Tang, B.-C. Chen, C. Cardie, S. Belongie, B. Hariharan, S.-N. Lim, Visual prompt tuning, in: *Proceedings of the 17th European Conference on Computer Vision*, Springer, 2022, pp. 709–727.

- [14] Z. Wang, Z. Zhang, C.-Y. Lee, H. Zhang, R. Sun, X. Ren, G. Su, V. Perot, J. Dy, T. Pfister, Learning to prompt for continual learning, in: Proceedings of the IEEE/CVF Conference on Computer Vision and Pattern Recognition, 2022, pp. 139–149.
- [15] J. Liang, D. Hu, Y. Wang, R. He, J. Feng, Source data-absent unsupervised domain adaptation through hypothesis transfer and labeling transfer, IEEE Transactions on Pattern Analysis and Machine Intelligence 44 (11) (2022) 8602–8617.
- [16] H. Zhang, M. Cissé, Y. N. Dauphin, D. Lopez-Paz, mixup: Beyond empirical risk minimization, in: Proceedings of the 6th International Conference on Learning Representations, 2018.
- [17] Y. Gan, Y. Bai, Y. Lou, X. Ma, R. Zhang, N. Shi, L. Luo, Decorate the newcomers: Visual domain prompt for continual test time adaptation, in: Proceedings of the AAAI Conference on Artificial Intelligence, Vol. 37, 2023, pp. 7595–7603.
- [18] S. Goyal, M. Sun, A. Raghunathan, J. Z. Kolter, Test time adaptation via conjugate pseudo-labels, Advances in Neural Information Processing Systems 35 (2022) 6204–6218.
- [19] M. Döbler, R. A. Marsden, B. Yang, Robust mean teacher for continual and gradual test-time adaptation, in: Proceedings of the IEEE/CVF Conference on Computer Vision and Pattern Recognition, 2023, pp. 7704–7714.
- [20] S. Niu, J. Wu, Y. Zhang, Z. Wen, Y. Chen, P. Zhao, M. Tan, Towards stable test-time adaptation in dynamic wild world, in: Proceedings of the 11th International Conference on Learning Representations, 2023.
- [21] G. Chakrabarty, M. Sreenivas, S. Biswase, SANTA: Source anchoring network and target alignment for continual test time adaptation, Transactions on Machine Learning Research (2023).
URL <https://openreview.net/forum?id=V7guVYzvE4>
- [22] A. Chaudhry, P. K. Dokania, T. Ajanthan, P. H. Torr, Riemannian walk for incremental learning: Understanding forgetting and intransigence, in: Proceedings of the European conference on computer vision, 2018, pp. 532–547.
- [23] A. Chaudhry, M. Rohrbach, M. Elhoseiny, T. Ajanthan, P. K. Dokania, P. H. Torr, M. Ranzato, On tiny episodic memories in continual learning, arXiv preprint arXiv:1902.10486 (2019).
- [24] H. Shin, J. K. Lee, J. Kim, J. Kim, Continual learning with deep generative replay, Advances in neural information processing systems 30 (2017).
- [25] A. A. Rusu, N. C. Rabinowitz, G. Desjardins, H. Soyer, J. Kirkpatrick, K. Kavukcuoglu, R. Pascanu, R. Hadsell, Progressive neural networks, arXiv preprint arXiv:1606.04671 (2016).
- [26] A. Mallya, D. Davis, S. Lazebnik, Piggyback: Adapting a single network to multiple tasks by learning to mask weights, in: Proceedings of the European conference on computer vision (ECCV), 2018, pp. 67–82.

- [27] Z. Wang, Z. Zhang, S. Ebrahimi, R. Sun, H. Zhang, C.-Y. Lee, X. Ren, G. Su, V. Perot, J. Dy, et al., Dualprompt: Complementary prompting for rehearsal-free continual learning, in: European Conference on Computer Vision, Springer, 2022, pp. 631–648.
- [28] P. Liu, W. Yuan, J. Fu, Z. Jiang, H. Hayashi, G. Neubig, Pre-train, prompt, and predict: A systematic survey of prompting methods in natural language processing, *ACM Computing Surveys* 55 (9) (2023) 1–35.
- [29] K. Zhou, J. Yang, C. C. Loy, Z. Liu, Learning to prompt for vision-language models, *International Journal of Computer Vision* 130 (9) (2022) 2337–2348.
- [30] A. Dosovitskiy, L. Beyer, A. Kolesnikov, D. Weissenborn, X. Zhai, T. Unterthiner, M. Dehghani, M. Mindler, G. Heigold, S. Gelly, J. Uszkoreit, N. Houlsby, An image is worth 16x16 words: Transformers for image recognition at scale, in: Proceedings of the 9th International Conference on Learning Representations, 2021.
- [31] M. U. Khattak, H. Rasheed, M. Maaz, S. Khan, F. S. Khan, Maple: Multi-modal prompt learning, in: Proceedings of the IEEE/CVF Conference on Computer Vision and Pattern Recognition, 2023, pp. 19113–19122.
- [32] J. Liu, R. Xu, S. Yang, R. Zhang, Q. Zhang, Z. Chen, Y. Guo, S. Zhang, Continual-mae: Adaptive distribution masked autoencoders for continual test-time adaptation, in: Proceedings of the IEEE/CVF Conference on Computer Vision and Pattern Recognition, 2024, pp. 28653–28663.
- [33] H. Xia, T. Jing, Z. Ding, Maximum structural generation discrepancy for unsupervised domain adaptation, *IEEE Transactions on Pattern Analysis and Machine Intelligence* 45 (3) (2022) 3434–3445.
- [34] C. Cui, F. Meng, C. Zhang, Z. Liu, L. Zhu, S. Gong, X. Lin, Adversarial source generation for source-free domain adaptation, *IEEE Transactions on Circuits and Systems for Video Technology* 34 (6) (2024) 4887–4898.
- [35] D. Hendrycks, T. Dietterich, Benchmarking neural network robustness to common corruptions and perturbations, in: Proceedings of the 7th International Conference on Learning Representations, 2019.
- [36] D. Hendrycks, S. Basart, N. Mu, S. Kadavath, F. Wang, E. Dorundo, R. Desai, T. Zhu, S. Parajuli, M. Guo, et al., The many faces of robustness: A critical analysis of out-of-distribution generalization, in: Proceedings of the IEEE/CVF international conference on computer vision, 2021, pp. 8340–8349.
- [37] Y. Yu, S. Shin, S. Back, M. Ko, S. Noh, K. Lee, Domain-specific block selection and paired-view pseudo-labeling for online test-time adaptation, in: Proceedings of the IEEE/CVF Conference on Computer Vision and Pattern Recognition, 2024, pp. 22723–22732.
- [38] B. Zhou, A. Khosla, A. Lapedriza, A. Oliva, A. Torralba, Learning deep features for discriminative localization, in: Proceedings of the IEEE conference on computer vision and pattern recognition, 2016, pp. 2921–2929.

- [39] Z. Gao, X.-Y. Zhang, C.-L. Liu, Unified entropy optimization for open-set test-time adaptation, in: Proceedings of the IEEE/CVF Conference on Computer Vision and Pattern Recognition, 2024, pp. 23975–23984.